

Analysis of optimal mixing in open-flow mixers with time-modulated vortex arrays

Bhargav Rallabandi,^{1,*} Cheng Wang,² and Sascha Hilgenfeldt^{3,†}

¹*Department of Mechanical and Aerospace Engineering, Princeton University, Princeton, New Jersey 08544, USA*

²*Department of Mechanical and Aerospace Engineering, Missouri University of Science and Technology, Rolla, Missouri 65409, USA*

³*Department of Mechanical Science and Engineering, University of Illinois at Urbana-Champaign, Urbana, Illinois 61801, USA*

(Received 22 December 2016; published 26 June 2017)

In this work, a systematic approach to efficient open flow mixing is introduced, using general theoretical concepts to identify optimized parameters of a deliberately introduced unsteady flow component. The method is applied in detail to two-dimensional (2D) advective mixing in flows resulting from the superposition of a transport flow through a channel and secondary localized cross-flows, here the vortical streaming due to a microbubble array. A simple description of stirring in a steady 2D vortex identifies the characteristic time beyond which vortex stirring becomes ineffective, with slow algebraic decay of the mix-variance. Duty cycling of the vortices introduces flow unsteadiness, for which optimum duty cycling protocols are identified, following analytically from a few selected Eulerian properties of the combined transport and vortex stirring flow. In comparison with experiments and simulations, it is shown that this simple formalism allows for the accurate prediction of optimal advective mixing, exponential in time, in the microbubble streaming case and, by extension, for any open-flow mixer with modulated secondary flow. Taking into account the effect of diffusion, estimated residence times required for complete mixing in such optimized devices are obtained.

DOI: [10.1103/PhysRevFluids.2.064501](https://doi.org/10.1103/PhysRevFluids.2.064501)

I. INTRODUCTION

Fluid mixing is a crucial part of many biological and industrial processes, where it is often desirable to homogenize two or more initially separate substances to aid a chemical reaction [1–3]. Mixing in general occurs as a combination of advection (stirring), which increases the surface area of contact between the two species by stretching and folding of fluid elements, and diffusion, which is ultimately responsible for homogenization at the molecular scale [4–6]. At macroscopic scales, fluid inertia allows the different species to continuously generate advective structures at small length scales (e.g., due to turbulence), which results in diffusion quickly homogenizing the mixture [7,8]. In most microfluidics applications, however, fluid inertia is negligible (small Reynolds numbers), making flows laminar [7,9,10], while the time required for mixing by diffusion alone over typical channel sizes used in microfluidics is prohibitively long for most applications [11]. The focus of mixing studies at the microscale has therefore been on tailoring protocols of *stirring* the fluid in order to establish advective patterns at finer length scales, which are then rapidly homogenized by diffusion [12–14]. Such optimal stirring protocols have been studied theoretically, focusing primarily on mixing in closed systems with zero throughput in often idealized situations (e.g., blinking vortices [15], linked-twist maps [16,17]).

*vbr@princeton.edu

†sascha@illinois.edu

Since it is usually desirable to have a continuous throughput through practical micromixing devices, the primary transport flow through the channel is augmented with secondary cross flows to obtain a flow with improved mixing properties. These cross flows are actuated either by geometric features built into the construction of the device (passive) [9,18,19] or by an external energy source (active) making use of driving forces such as dielectrophoresis or thermal currents [7,20,21]. In many cases, the cross flows are locally actuated and therefore have decaying flow strength away from the actuator, resulting in vortical flow structures [7,9]. Such vortical cross flows can be produced by a number of actuation methods, e.g., using high-frequency acoustics (including surface acoustic waves) [22–26] or electrokinetics [27–29].

The strength of the cross flow relative to the transport flow determines the topology of the resulting flow and thereby its mixing properties. Weak cross flows only slightly modify the flow pattern and allow continuous transport of fluid elements through the device, but at the cost of long mixing times and channel lengths. By contrast, strong cross flows establish local vortex patterns, which offer better mixing capabilities but invariably establish localized recirculation regions, preventing mixed fluid from being efficiently transported through the channel. This makes it necessary to actively modulate the secondary flow to achieve rapid mixing at a high throughput.

Which temporal modulation protocol yields optimal results for a given open-flow vortex mixer? This question has not been addressed systematically, and it is the main focus of the present study to identify optimal protocols of engineering flow unsteadiness through duty cycling, providing useful guidelines for the design of efficient mixing devices. Using general physical and geometric arguments, we develop a theoretical framework that identifies both the optimal duty cycle and the maximal mixing rate as a function of the properties of the vortices and the throughput through the channel. These theoretical arguments are applied to the specific case of a microbubble mixing array, where they are shown to be in quantitative agreement with both experiments and simulations of mixing. The theoretical framework is not tied to a specific driving mechanism or flow and thus provides general rules to optimize unsteadiness open flow micromixers with vortical cross flows. The generality of the approach will be emphasized throughout the subsequent development.

The setup and methods are described in Sec. II. In Sec. III we first quantify some features of mixing without time modulation; while the mixing in this case is poor, this analysis provides us with the length and time scales that are crucial to designing optimum time-modulated mixers. We then demonstrate that the introduction of unsteadiness by means of duty cycling of the vortices results in exponentially fast mixing. Using simple physical and geometric arguments, we develop a general theoretical framework that predicts both the optimal duty cycle pattern and the rate of mixing. Through experimental data and numerical simulations, we then demonstrate that the theory quantitatively predicts the optimal mixing protocol. We then estimate the typical residence time in the mixer before diffusion homogenizes the mixture; Sec. IV presents conclusions.

II. SETUP AND METHODS

While the physical arguments for optimal mixing that we develop are generally applicable to vortical flows, it is useful to discuss the general ideas applied to a concrete problem, in particular to validate the arguments against the results of experiments and numerical simulations. As a model vortex-based micromixer in which the fluid flow is well understood theoretically and experimentally, we consider here an array of acoustically excited microbubbles attached to the walls of a microchannel. This type of device is known as a simple and robust method of microfluidic flow actuation, in which applied acoustic energy (at ultrasound frequencies) is rectified into a powerful steady streaming flow. Ease of manufacture and actuation makes bubble-based devices particularly attractive for microfluidics, where they have been utilized for a variety of applications such as shear force actuation [30], particle trapping and focusing [31,32], size sorting [33], and fluid mixing [34–37]. Such microbubble-driven flows are well understood analytically [33,38] and have been shown to lend themselves well to temporal modulation [36,39] by tuning the driving amplitude.

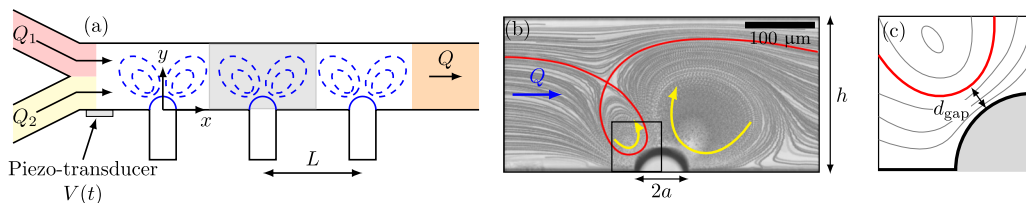


FIG. 1. (a) Typical open flow micromixer design showing inlets from which initially unmixed fluid streams are introduced towards an array of actuators—here acoustically excited microbubbles—located in the main channel a distance $L = 2h$ apart. The ultrasound drives vortical microbubble streaming flow whose strength may be temporally modulated by applying a time-dependent voltage amplitude to the piezo-transducer. (b) Path lines of the typical 2D flow around a bubble [region shaded gray in (a)] resulting from an excitation of the streaming in the presence of a finite flow rate Q through the channel. The flow consists of both open and closed regions (upstream and downstream vortices) divided by a separatrix (red solid line). (c) Schematic of a close-up of the square box in (b): Much of the incoming flow is funneled into a narrow gap of width d_{gap} between the bubble surface and the separatrix, where diffusive mixing is important at long times. The bubble radius is $a = 40 \mu\text{m}$, and the channel height $h = 250 \mu\text{m}$ in experiments.

The geometry of the setup considered here for open-flow micromixing is illustrated in Fig. 1(a), indicating the location of an array of bubbles relative to the inlets and outlets of the microfluidic channel. The bubbles are attached to a wall of the microchannel by means of blind side channels of width $2a$, which protrude from the main channel. The main channel has a rectangular cross section with a height h in the y direction [indicated in Fig. 1(b)] and a depth d (not shown). The rectangular geometry of the side channel establishes a bubble of semicylindrical shape (semicircular cross section), of radius a and whose cylindrical axis spans the entire channel depth d . The bubble-to-bubble distance in our experiments along the x axis is $L = 2h$. Figure 1 shows a representative cross section of the channel perpendicular to the bubble axis.

The application of ultrasound at a frequency $f \sim 1\text{--}100$ kHz establishes oscillations of the bubble interface with a characteristic amplitude ϵa , which, through a rectification of the acoustic energy, drives a secondary *steady* flow (streaming) with a characteristic speed $u_s = 2\pi\epsilon^2 a f$. Due to the cylindrical symmetry of the bubble, the streaming is approximately confined to cross-sectional planes perpendicular to the bubble axis [two-dimensional (2D) flow] and is characterized by a pair of steady counter-rotating vortices [36,38,40]. In addition to the streaming, there is a net transport of fluid through the channel due to an imposed transport (Poiseuille) flow with a volumetric flow rate Q . The net flow resulting from the steady combination of the Poiseuille flow through the channel and the bubble-driven streaming consists of regions of open streamlines in addition to closed upstream and downstream vortices, as shown in Fig. 1(b); the majority of the total flow rate is forced through a thin gap between bubble surface and upstream vortex [Fig. 1(c)], a feature important for the action of diffusion; cf. Sec. III E. Similar flow structures have been obtained using other actuation methods, e.g., using surface acoustic waves [25] or electroconvection [41].

A. Experiments

The microbubble-based mixing devices are fabricated in polydimethylsiloxane using standard soft lithography techniques [42], described in more detail elsewhere [39]. We use a T-shaped microfluidic mixer structure that consists of a main channel of height $h = 250 \mu\text{m}$ and depth $d = 100 \mu\text{m}$, two inlets, and one or more side channels, which are either all on the same side of the main channel [as in Fig. 1(a)] or staggered [alternating on opposite sides; cf. Fig. 2(a) for an experimental image].

When liquids are introduced from the inlets, air is trapped inside the side channels automatically forming semicylindrical bubbles of the type discussed above. Microbubbles in planar microfluidic devices like these are often used to generate steady streaming flows of approximately 2D character

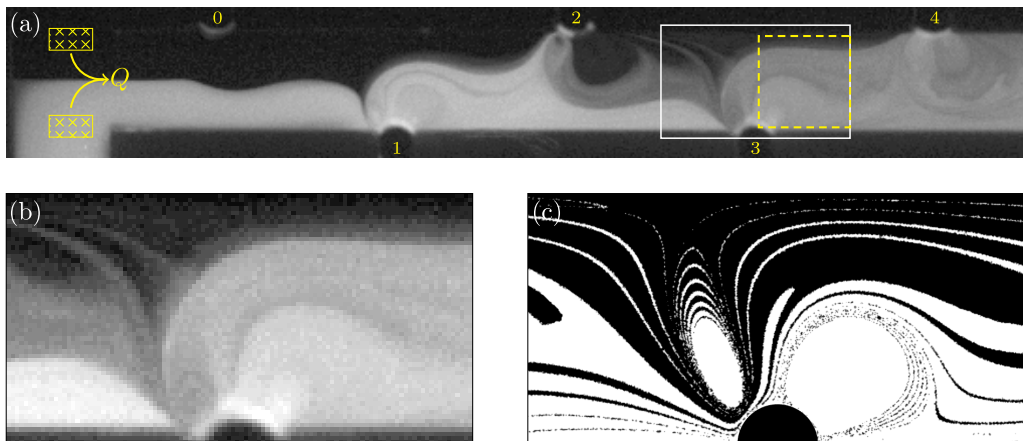


FIG. 2. Mixing in a superposition of steady transport flow and steady bubble streaming [cf. Fig. 1(c)] in a staggered microbubble array. (a) Experiment with fluorescent nanoparticles, brightness indicating local particle concentration. The fluorescence intensities of the bright and dark streams before they meet (respectively C_{\max} and C_{\min}) are evaluated in the regions enclosed by shaded rectangles and are used to compute the normalized intensity $c(\mathbf{x}, t)$ in experiments. The dashed square indicates a region of interest for the evaluation of Φ^2 and is typically located downstream of the bubble and spans all or most of the channel height. (b) Mixing field within the white rectangle indicated in (a) around the bubble labeled 3. (c) Mixing simulation by Lagrangian particle advection at infinite Pe with periodic boundary conditions at a time $t = 2 \times (2h) / \bar{u}_p$. This is the mean transport time between the bubbles labeled 1 and 3 in (a) and hence serves as the numerical counterpart of (b); note that the bubble labeled 0 in the experiment does not get excited by the ultrasound (possibly due to its proximity to the corners of the geometry). The finer structures in (c) do not appear in (b) partly due to limited optical resolution and partly due to diffusive mixing.

[31], greatly improving the ability to both quantitatively control and quantitatively predict the flow [32,36,38].

A syringe pump is used to infuse two liquid streams through the two inlets; one liquid stream is DI water containing fluorescent polystyrene particles (radius $a_p = 50$ nm, Life Technologies), the other stream consists of the same fluid but without fluorescent particles. Each stream has equal flow rate $Q/2$. We use a mercury-vapor lamp as the light source through an epi-fluorescence attachment, with excitation and emission filter wavelengths of ≈ 460 nm and ≈ 520 nm, respectively. Under the illumination, the emission from the fluorescent particles is captured and recorded by a high-speed camera. In the range of particle concentrations employed in our experiments ($\leq 1\%$ by volume), the gray scale intensity (fluorescent signal C) of the image is proportional to the particle concentration in the liquid [43,44], so that the fluorescent signal distribution quantifies mixing of the particles, as in many other studies [43,45,46].

The Stokes-Einstein diffusion coefficient of the nanoparticles in a fluid of dynamic viscosity μ is $D_p = k_B T / (6\pi \mu a_p) \approx 1.6 \times 10^{-12} \text{ m}^2 \text{ s}^{-1}$, and the diffusion time scale across the channel height can be estimated as $t_d \sim h^2 / (4D_p) \approx 10^4 \text{ s}$. The residence time of a patch of fluid in the device is typically a few seconds in the present experimental setups, much shorter than the time required for mixing by diffusion alone. Thus, choosing nanoparticles rather than more rapidly diffusing dye molecules allows us to evaluate and optimize the mixing effect of the bubble streaming flow field due to advection alone, independent of diffusive effects. The iterative (and optimized) application of modulated streaming flow will eventually lead to characteristic length scales of particle concentration patterns small enough for diffusion to become effective (cf. Sec. III E).

B. Flow field and mixing simulations

We are interested in the general mixing properties of the combination of a Poiseuille flow (transport) and a vortex flow (streaming). For a kinematic viscosity ν of the fluid, the maximal streaming Reynolds number $\text{Re}_s \equiv u_s a / \nu$ (corresponding to flow speeds very close to the bubble) is typically in the range $0.3 \lesssim \text{Re}_s \lesssim 7$, while flow speeds decay strongly at larger distances to the bubble surface [38]. The streaming flow is well described by leading order theory ($\text{Re}_s \rightarrow 0$) up to $\text{Re}_p \lesssim O(10)$, suggesting that the inertia of the steady streaming plays only a small role under typical experimental conditions [47]. The Reynolds number associated with the Poiseuille flow $\text{Re}_p \equiv Q/(hd) \times h/\nu$ (corresponding to gradients on scale of the channel height) is typically $O(0.01)$. The net flow can therefore be accurately quantified by a linear superposition of the individual flows, as confirmed in Ref. [33].

The cylindrical bubble geometry causes the secondary flow to be approximately 2D in the xy planes perpendicular to the bubble axis; see Fig. 1(b). The 2D streaming velocity field $\mathbf{u}_s(x, y)$ has been determined analytically for wide channels $h/a \gg 1$ [38] and can be generalized to channels of finite height h using a rapidly converging iterative semianalytical formalism [33]. The Poiseuille flow velocity profile $u_x(y, z)$ for a given flow rate Q in a channel of height h and depth d in the absence of a bubble can be expressed as $\mathbf{u}_p^\infty = u_p^\infty(y, z)\mathbf{e}_x$, where [48]

$$u_p^\infty(y, z) = Q \left(\sum_{n \text{ odd}} \frac{2}{n^4 \pi} \left\{ 1 - \frac{\tanh[n\pi d/(2h)]}{2h/(n\pi d)} \right\} \right)^{-1} \sum_{n \text{ odd}} \frac{1}{n^3} \left\{ 1 - \frac{\cosh(n\pi z/h)}{\cosh[n\pi d/(2h)]} \right\} \sin\left(\frac{n\pi y}{h}\right). \quad (1)$$

The presence of the bubble modifies this flow (for example, by introducing velocity components in y), which now also has to satisfy conditions of zero normal velocity and zero tangential stress at the bubble surface. This modification may be effected using a similar procedure as that used for the streaming and is detailed in Ref. [33]. The resulting modified Poiseuille flow in the $z = 0$ plane is then specified for some flow rate Q by the 2D incompressible velocity field $\mathbf{u}_p(x, y)$. The superposition of the streaming and Poiseuille flows in $z = 0$ results in the 2D flow field $\mathbf{u}(\mathbf{x}) = (u(x, y), v(x, y))$, which can be written as

$$\mathbf{u}(\mathbf{x}) = \mathbf{u}_s(\mathbf{x}) + \mathbf{u}_p(\mathbf{x}). \quad (2)$$

We stress that this flow field description is not the result of a numerical simulation, but of a finite summation of analytically known terms. Therefore, we can describe the entire class of combined streaming-transport flows by a small number of well-defined parameters. More generally, \mathbf{u}_s is a general vortical flow that is known either analytically or numerically.

We define u_{\max} as the maximum speed of the streaming flow (i.e., the maximum over \mathbf{x} of $|\mathbf{u}_s|$), invariably attained at the bubble surface and related to u_s by $u_{\max} = \beta u_s$, where the $O(1)$ prefactor β is a known function of the driving frequency [33,49]; e.g., for $f \approx 21.9$ kHz, $\beta \approx 1.8$. The mean Poiseuille flow speed in the $z = 0$ plane \bar{u}_p is

$$\bar{u}_p \equiv \frac{1}{h} \int_0^h u_p^\infty|_{z=0} dy, \quad (3)$$

where we have used the fact that far from the bubble, the flow approaches \mathbf{u}_p^∞ . For the channel geometry considered here ($d/h = 0.4$), one finds from (1) that $\bar{u}_p \approx 1.48 Q/(hd)$. The relative strength between the Poiseuille and streaming flows is quantified by $s \equiv \bar{u}_p/u_{\max}$. The parameter s is easily controlled in experiment either by modifying the voltage of the ultrasound that drives the streaming (since $u_{\max} = 2\pi \epsilon^2 a f \beta$) or by adjusting the flow rate Q of the Poiseuille flow through the micromixer [31,33]. The 2D flow $\mathbf{u}(\mathbf{x})$ can otherwise be written in terms of a stream function ψ defined by $\psi = \int u dy = -\int v dx$, which will prove useful in subsequent sections. The structure of the flow discussed thus far is generally applicable to 2D (or nearly 2D) vortex flows excited by local actuating elements and is not specific to microbubble streaming.

On an open streamline within the combined streaming and transport flow (2), a fluid element is forced through a thin gap between the bubble surface and the upstream vortex [31–33] [see Fig. 1(c)]. By continuity, this gap has thickness $d_{gap} \approx sh$ [31], and we will show that it ultimately plays a role in diffusive mixing; see Sec. III E.

The mixing under the flow field $\mathbf{u}(\mathbf{x})$ is quantified by the spatial structure of a spatio-temporally evolving scalar field $c(\mathbf{x}, t)$ that describes the concentration of a species that is advected in the flow. Defining a dimensionless position, velocity, and time $\tilde{\mathbf{x}} = \mathbf{x}/h$, $\tilde{\mathbf{u}} = \mathbf{u}/\bar{u}_p$, and $\tilde{t} = t/(h/\bar{u}_p)$ (t represents the dimensional time), respectively, and a dimensionless gradient operator $\tilde{\nabla} = h\nabla$, a passive scalar field c satisfies

$$\frac{\partial c}{\partial \tilde{t}} + (\tilde{\mathbf{u}} \cdot \tilde{\nabla})c = \frac{1}{\text{Pe}} \tilde{\nabla}^2 c, \quad (4)$$

subject to initial and boundary conditions on c . The Péclet number $\text{Pe} \equiv \bar{u}_p h / D_p$ is large in our experiments ($\gtrsim 10^5$), a consequence of the use of nanoparticles to suppress diffusive mixing versus advective stirring (see above). As a first approximation, we therefore neglect diffusive effects entirely and consider advective mixing (stirring) only, i.e., $\text{Pe} \rightarrow \infty$.

The advection equation in general does not admit simple analytical solutions and is not straightforward to solve numerically using grid-based techniques due to the continuous refinement of advected structures. To accurately solve (4) in the $\text{Pe} \rightarrow \infty$ limit, we use a Lagrangian particle method, where we compute the advection of a large number of passive tracers in the flow, by solving $d/dt[\mathbf{x}_i(t)] = \mathbf{u}[\mathbf{x}_i(t)]$ for the positions $\mathbf{x}_i(t)$ of individual tracers i . Each tracer is identified with a value of the scalar field, which therefore also advects passively with the tracers. The scalar field is reconstructed at any instant of time by a linear interpolation of the values assigned to the tracers onto a Cartesian grid. This technique, especially suited to problems with negligible diffusion, has been widely employed in previous mixing studies to good effect [50–52]. We initialize the simulations with uniformly spaced tracers at a density of 512^2 tracers per $h \times h$ region of the spatial domain. The trajectories of the tracers are then computed numerically using a fourth-order Runge-Kutta scheme. The numerical results presented in subsequent sections are verified to be convergent with respect to tracer density and the time step of the integration.

C. Quantification of mixing effectiveness

The quality of mixing at an instant of time is directly related to the spatial distribution of the instantaneous scalar field $c(\mathbf{x}, t)$ that is passively advected by the flow. To quantify the mixing quality we use the mix-variance of c , which is a multiscale mixing measure appropriate for 2D advection-dominated flows [53,54]. The mix-variance of a scalar field $c(\mathbf{x}, t)$, denoted by $\Phi^2(c - \bar{c})$, is defined as

$$\Phi^2(c - \bar{c}) = \sum_{\substack{\mathbf{k} \\ |\mathbf{k}| \neq 0}} \Lambda_{\mathbf{k}} |\hat{c}_{\mathbf{k}}|^2, \quad \text{with} \quad \Lambda_{\mathbf{k}} = [1 + (2\pi |\mathbf{k}|)^2]^{-1/2}. \quad (5)$$

The $\hat{c}_{\mathbf{k}}$ are 2D Fourier components of $c(\mathbf{x})$, defined as

$$\hat{c}_{\mathbf{k}}(t) = \int_{\text{ROI}} c(\mathbf{x}', t) e^{-i2\pi \mathbf{k} \cdot \mathbf{x}'} d^2 \mathbf{x}', \quad (6)$$

where $\mathbf{x}' = (x', y')$ is a rescaled position vector, with $x', y' \in [0, 1]$ within the region of interest (ROI). The omission of the $\mathbf{k} = \mathbf{0}$ Fourier mode in (5) ensures that the mean value \bar{c} of $c(\mathbf{x})$ does not influence the value of Φ^2 . The mix-variance is particularly useful in the limit of $\text{Pe} \rightarrow \infty$, since it penalizes the spectral energy contributions contained in shorter wavelengths by the weight factor $\Lambda_{\mathbf{k}}$ (lower values of Φ^2 indicate better mixing). We point out here that Φ^2 has units of length (via $\Lambda_{\mathbf{k}}$), whose value is representative of a characteristic length scale of variation of the scalar field c . We additionally rescale Φ^2 by its initial value Φ_0^2 to obtain a normalized mixing measure $\phi^2(t) \equiv \Phi^2/\Phi_0^2$ which varies between 1 (the initial, fully unmixed state) and 0 (fully mixed).

In our mixing experiments, the gray scale fluorescent intensities of the two liquid streams before they meet at the junction [cf. Fig. 2(a)] are denoted, respectively, by C_{\max} and C_{\min} for the bright (containing fluorescent nanoparticles) and dark streams. We normalize the intensity field $C(\mathbf{x}, t)$ as $c(\mathbf{x}, t) \equiv [C(\mathbf{x}, t) - C_{\min}]/(C_{\max} - C_{\min})$, so that in the unmixed state, the bright and dark streams are identified with $c = 1$ and $c = 0$, respectively. In both experiments and simulations, we typically select a square ROI located just downstream of the bubble and covering most of the channel height; cf. Fig. 2(a). To compute the mix-variance, x and y are rescaled by the dimensions of the ROI so that (5) can be applied directly.

We restrict our attention to the experimentally relevant initial distribution of the scalar field $c(\mathbf{x})$ characterized by two distinct layers of unmixed fluid separated by a sharp interface of contact, located initially at $y = y_0$. The initial distribution of the scalar field is therefore

$$c(\mathbf{x}, t = 0) = c_0(\mathbf{x}) = H(y_0 - y), \quad (7)$$

where $H(\cdot)$ is the Heaviside function. In experiments, where the initially unmixed fluids are introduced from the two different inlets [Fig. 2(a)], y_0 is determined by the ratio of flow rates through the two inlets. Here we consider equal flow rates, so that $y_0 = h/2$.

III. RESULTS AND DISCUSSION

The superposition of Poiseuille transport flow and vortex flow is prototypical for a practical open flow mixer, where a constant throughput has to be reconciled with mixing action induced by a secondary flow (here the vortices). If the secondary flow is weak, no mixing effects beyond Taylor–Aris dispersion due the transport flow [55,56] are expected, so that we focus here on situations where the streaming is strong relative to the transport, i.e., $s \ll 1$. This ensures both greater flow speeds near the bubbles and greater coverage of the mixing volume by the vortices.

However, a mere steady superposition with the vortex flow will simply modify the streamlines of the transport flow, and any mixing efficiency is severely limited through the Poincaré–Bendixson theorem, which disallows chaotic advection in 2D steady flows [57]. It is therefore critical that the flow be modulated in order to utilize the flow effectively.

A. Mixing on open streamlines versus vortex mixing

Before modulation is applied, it is crucial to quantify the mixing action of the steady flow in both open-flow (transport) and closed-streamline (vortex) regions. In the $Pe \rightarrow \infty$ limit, this requires computing the stretching of striation filaments of the concentration field. The efficacy of this stretching depends on the characteristic local strain rate of the flow, given by $\dot{\gamma} = (\mathbf{E} : \mathbf{E})^{1/2}$, where $\mathbf{E} \equiv \frac{1}{2}(\nabla \mathbf{u} + \nabla \mathbf{u}^T)$ is the rate-of-strain tensor.

We shall first show that the average strain rates a fluid particle experiences within a vortex are greater than those in the open-streamline transport flow. Note that both vortex trajectories and open trajectories are periodic in a bubble array as in Fig. 1(a). A quick estimate shows that the accumulated strain on open streamlines over one period is $O(1)$: this is obviously true in the undisturbed Poiseuille flow between bubbles, where $\dot{\gamma} \sim (\bar{u}_p/h)$ and transport times from bubble to bubble ($L \sim h$) are $\sim h/\bar{u}_p$. Likewise, in the thin gap flow [cf. Fig. 1(c)] directly next to the bubble, the flow speed is a factor $1/s$ greater and flow gradients are set by the bubble radius a , so that $\dot{\gamma} \sim \bar{u}_p/(sa)$, while the transport through the gap takes a time $\sim (sa)/\bar{u}_p$. Misorientation of the striation elements will further limit the efficacy and the total stretch, but the order of magnitude of the average strain rate is $\chi_o \sim \bar{u}_p/h \sim su_s/h$.

By contrast, fluid elements within the vortices are more effectively stretched, mostly because the net shear strain rate across streamlines is much larger. The mean shear rate experienced by a fluid

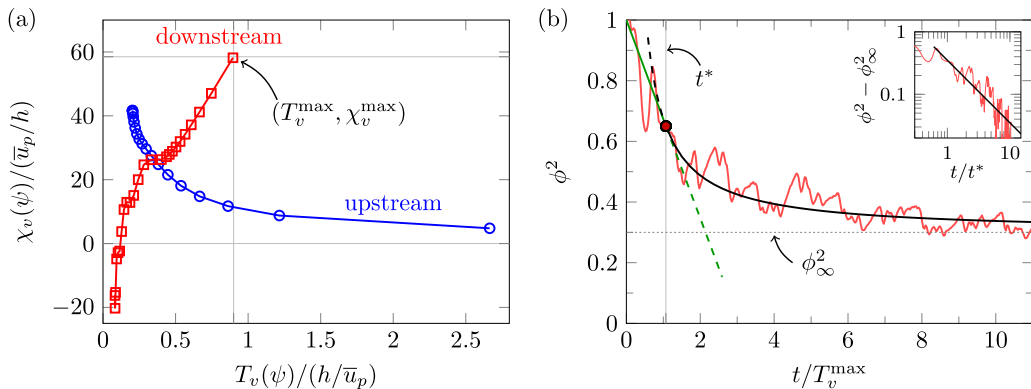


FIG. 3. (a) Mean shear rates $\chi_v(\psi)$ versus orbit times $T_v(\psi)$ in upstream and downstream vortices. The outermost streamline of the downstream vortex has the largest shear rate χ_v and an orbit time $T_v^{\max} \approx 0.89h/\bar{u}_p$ for $s = 0.02$. (b) Normalized mix-variance $\phi^2(t)$ for steady mixing in a microbubble array (see Fig. 2) computed from a simulation (red). The expression (9) predicts a linear decay for short times $t < t^*$ (green) and decays as t^{-1} to ϕ_∞^2 at long times $t > t^*$ (black); here $t^* \approx 1.07 T_v^{\max}$ and $\phi_\infty^2 \approx 0.3$ are obtained by a fit of (9) to the simulation data. We find that $t^* \approx T_v^{\max}$ over a wide range of initial conditions, indicating that the decay of ϕ^2 becomes considerably slower for $t \gtrsim T_v^{\max}$ and suggesting an optimum stirring time $t^* \approx T_v^{\max}$. The inset shows the t^{-1} decay of $\phi^2 - \phi_\infty^2$ at long times. The results pertain to $f = 21.9$ kHz and $s = 0.02$.

element as it completes a closed streamline orbit (stream function ψ) is

$$\chi_v(\psi) \equiv \frac{1}{T_v(\psi)} \int_t^{t+T_v(\psi)} \mathbf{n} \cdot 2\mathbf{E} \cdot \mathbf{s} dt, \quad (8)$$

where $\mathbf{s} = \mathbf{u}/|\mathbf{u}|$ and $\mathbf{n} = \mathbf{s} \times \mathbf{e}_z$ are the unit tangent and normal vectors to the motion of the element on ψ , respectively, and $T_v(\psi) \equiv \oint_\psi \mathbf{s} \cdot d\mathbf{x}/|\mathbf{u}|$ is the orbit time by definition. Figure 3(a) shows $\chi_v(\psi)$ for the upstream and downstream vortices in units of \bar{u}_p/h , for a theoretically computed flow field with parameters representative of bubble microstreaming experiments. As expected, the values of $\chi_v(\psi)$ are a factor $1/s \gg 1$ larger than χ_o (i.e., $\chi_v \sim u_s/a$); similar reasoning holds in devices utilizing different secondary flow fields than bubble streaming vortices. This clarifies that any optimization of mixing action must focus on the vortex flow.

B. Optimizing vortex mixing

From its initial value of Φ_0^2 , the mix-variance of a bright-dark concentration pattern of striations in a vortex decreases with exposure time to the vortex flow. Initially (by continuity), this decay is linear, but for long times (again in the limit $\text{Pe} \rightarrow \infty$), a universal asymptotic behavior takes over: In steady 2D shear flow, the fluid element stretch becomes linear in time under general assumptions; equivalently, the thickness of striations in the bright-dark concentration pattern decays as t^{-1} [2]. This algebraic t^{-1} decay is inherited by Φ^2 , and demonstrates that 2D steady flows are poor mixers compared to flow fields that lead to exponential decay of striation thickness or Φ^2 , usually considered the hallmark of successful mixing [2,53]. Depending on the initial distribution of striations and the details of the steady 2D flow, parts of the scalar field can remain unmixed even at long times (e.g., close to stagnation points or no-slip walls) in the absence of diffusion. These unmixed regions cause the decay of Φ^2 to, in general, approach a nonzero asymptotic value Φ_∞^2 , so that $\Phi^2 \sim \Phi_\infty^2 + O(t^{-1})$ for long times, further limiting the efficacy of steady vortices for mixing. The persistence of unmixed regions and t^{-1} decay of striation thicknesses outside these regions are general features of advective mixing in 2D steady flows [4,58].

Matching both the values and the decay rates of the generic short- and long-time asymptotes of $\Phi^2(t)$ [$\Phi^2(t) \sim \Phi_0^2 - b_1 t$ and $\Phi^2(t) \sim \Phi_\infty^2 + b_2 t^{-1}$, respectively, with b_1 and b_2 being determined

by the details of the flow] at an intermediate time t^* , the mix-variance in a steady vortex can be expressed as a piecewise C^1 continuous function

$$\phi^2(t) \equiv \frac{\Phi^2(t)}{\Phi_0^2} \approx \begin{cases} 1 - (1 - \phi_\infty^2) \frac{t}{2t^*}, & t \lesssim t^* \\ \phi_\infty^2 + (1 - \phi_\infty^2) \frac{t}{2t^*}, & t \gtrsim t^*, \end{cases} \quad (9)$$

where $\phi_\infty^2 \equiv \Phi_\infty^2 / \Phi_0^2$. In this expression, the details of the flow field and the initial conditions are contained entirely within the parameters t^* and ϕ_∞^2 . Figure 3(b) demonstrates this conclusion for the striation pattern inside the downstream vortex: aside from periodic modulations due to initial distribution within the vortex, ϕ^2 shows a crossover well fit by (9). Of particular importance is the crossover time t^* in (9), which represents the time beyond which mixing inside the vortex flow becomes less efficient (per time). It is useful from a practical standpoint to estimate t^* using the kinematic properties of the flow field, rather than requiring a full solution of (4).

In our example, as in many open-flow mixers, the flow is very inhomogeneous within each vortex, with the greatest average strain rate χ_v^{\max} applied in the downstream vortex close to the bubble and therefore on streamlines at the outer edge of this vortex [cf. Fig. 3(a) and (8)]. In order for every fluid element on this outermost streamline (we denote its stream function by ψ^{\max}) to experience $\chi_v^{\max} = \chi_v(\psi^{\max})$, the vortex flow needs to act for a duration $T_v^{\max} = T(\psi^{\max})$. Note that $T(\psi_{\max}) = \max[T(\psi)]$, so that all fluid elements in the downstream vortex complete at least one orbit during this time. It is thus reasonable to estimate the crossover time as $t^* = T_v^{\max}$, which is confirmed by steady simulations, where we find $t^*/T_v^{\max} = 1.07$; cf. Fig. 3(b). Stirring fluid elements in the vortex beyond $t = t^*$ becomes less and less efficient, and the mixed fluid in the vortex is of course never transported downstream. In general, the inefficiency of 2D steady mixing arises from the gradual orientation of striations along streamlines by the flow [4,58] (which occurs here on the time scale t^*). For these reasons, it is necessary to modulate the flow on time scales $t \sim t^*$ in order to overcome these limitations.

The theoretical arguments that lead to (9) follow from the general properties of passive advection in vortices and are not tied to the specific structure of the bubble streaming flow. In particular, a maximally shearing streamline with an orbit time of T_v^{\max} can be found for any set of closed streamlines. If this maximally shearing orbit is sufficiently large (as is the case here), it dominates the stirring properties of the entire vortex so that $t^* \approx T_v^{\max}$ in (9). Note that at the crossover time $t = t^*$, we find from (9) that $\phi^2 = \frac{1}{2}(1 + \phi_\infty^2)$. The value of ϕ_∞^2 depends on the initial conditions presented to the vortical flow, although its precise value is unimportant for our purposes, as we will show in the following sections.

C. Flow modulation by duty cycling

The slow algebraic t^{-1} decay of mixing measures in steady vortex flows can be overcome by the deliberate introduction of unsteadiness. A practical flow modulation strategy at constant throughput (steady Poiseuille flow) is duty cycling of the streaming, which has the benefit of requiring only relatively simple control of the vortex strengths, and is readily generalizable to other kinds of cross flows.

For microbubble streaming, this is effected simply by alternately turning on and off the ultrasound for time intervals τ_{on} and τ_{off} respectively. Transients during the on-off process can be neglected by ensuring that the frequency of the modulation is much smaller than that of the ultrasound ($\tau_{\text{on}}, \tau_{\text{off}} \gg 1/f$). For our mixing simulations, we use the time periodic flow field (with period $\tau_{\text{cycle}} \equiv \tau_{\text{on}} + \tau_{\text{off}}$) defined by

$$\mathbf{u} = \begin{cases} \mathbf{u}_p + \mathbf{u}_s, & 0 < t < \tau_{\text{on}}, \\ \mathbf{u}_p, & \tau_{\text{on}} < t < \tau_{\text{cycle}}, \end{cases} \quad (10)$$

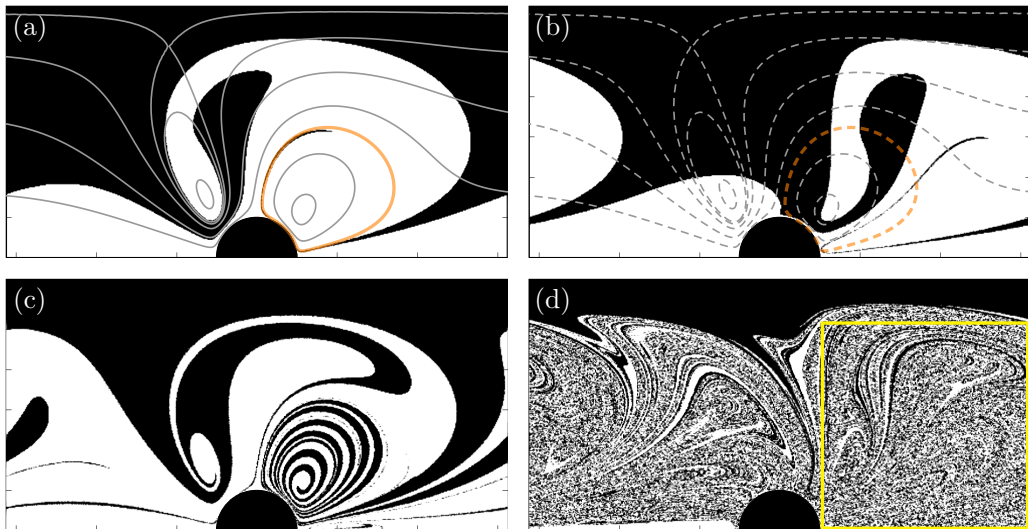


FIG. 4. Snapshots of the scalar field mixing due to a duty cycle with $\tau_{\text{on}} = \tau_{\text{off}} = 0.4h/\bar{u}_p$, at different instants of time: (a) at the end of “on” part of the first cycle, $t = \tau_{\text{on}}$, (b) at the end of the first cycle, $t = \tau_{\text{cycle}}$, (c) at the end of the “on” part of the second cycle, $t = \tau_{\text{cycle}} + \tau_{\text{on}}$, and (d) after eight cycles, $t = 8\tau_{\text{cycle}}$. Streamlines of the superposition $\mathbf{u}_p + \mathbf{u}_s$ are indicated in (a) and (b), with the outermost streamline of the downstream vortex indicated in orange. Partially stirred fluid during the “on” part of the cycle due to the flow $\mathbf{u}_p + \mathbf{u}_s$ [cf. panel (a)] is advected during the “off” part of the cycle by the transport flow \mathbf{u}_p . By the end of a full cycle (b), the scalar field has been favorably redistributed for stirring during the next “on” phase, whose streamlines are here indicated as dashed lines. Iterative application of the duty cycle results in efficient mixing.

where t is defined modulo τ_{cycle} . The simulation also uses periodic boundary conditions at $x = \pm h$, corresponding to a bubble array with the experimental spacing $L = 2h$.

During the “on” phase of the cycle, mixing proceeds as indicated above, primarily in the closed upstream and downstream vortices of the flow. During the “off” phase, these mixed regions of fluid are transported downstream by the Poiseuille flow, presenting a rearranged advection field to the next “on” phase of the cycle. This rearrangement of the advection field allows the vortices during the “on” phase of the next cycle to stretch and fold new material, further refining the advection field.

In a periodic bubble array, a given volume of fluid is deformed repeatedly during several cycles. Figure 4 shows a simulation of the successive refinement of fluid passing periodically by a bubble streaming element under duty cycling. In Fig. 5 we plot the Φ^2 values associated with this process [computed from the numerical solution for $c(\mathbf{x}, t)$] and show that Φ^2 now decays *exponentially* with time in the mean. This dramatic improvement demonstrates that the modulation allows fluid elements to experience comparable *factors* of decrease in ϕ^2 during every cycle, thus achieving the signature exponential decay associated with efficient stretching and folding [2,54,59].

More formally, the relative mix-variance is found to oscillate (with period τ_{cycle}) about a mean exponential trend of the form

$$\phi^2(t) \equiv \frac{\Phi^2(t)}{\Phi_0^2} = \alpha e^{-\sigma t/\tau_{\text{cycle}}}, \quad \text{for } t \gg \tau_{\text{cycle}}. \quad (11)$$

Here $\alpha(\tau_{\text{on}}, \tau_{\text{off}})$ and $\sigma(\tau_{\text{on}}, \tau_{\text{off}})$ are respectively an $O(1)$ prefactor and an exponential rate constant that depend on the duty cycle and are obtained by a least-squares fit to the result of the simulation. The value of $\alpha(\tau_{\text{on}}, \tau_{\text{off}})$ is relatively insensitive to the duty cycle chosen and is close to unity. However, due to the exponential decay of ϕ^2 , it is worthwhile identifying optimum combinations of τ_{on} and τ_{off} (duty cycling protocols) that maximize σ .

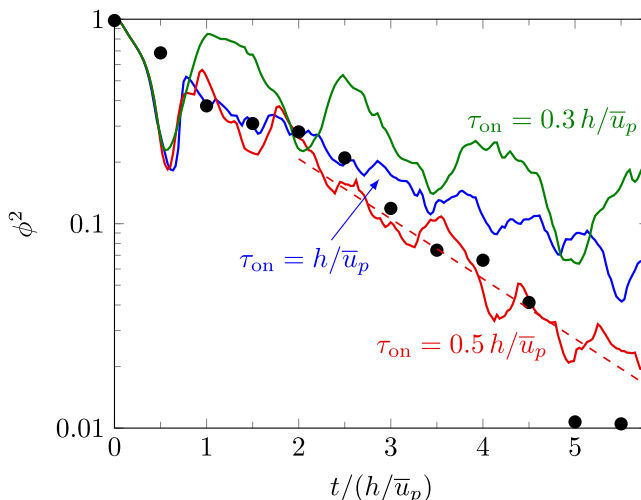


FIG. 5. Decay of the normalized mix-variance $\phi^2 = \Phi^2/\Phi_0^2$ under duty cycling for an array of bubbles showing results of simulations (lines) and an experiment (markers). Simulations correspond to duty cycles with a constant $\tau_{off} = 0.4h/\bar{u}_p$ and varying τ_{on} and use periodic boundary conditions. Experimental markers correspond to a 50% duty cycle with $\tau_{on} = \tau_{off} = 0.36h/\bar{u}_p$ in a bubble array similar to Fig. 2(a). The distance X along the array in experiments is used as a proxy for time t in simulations using the mean transport speed \bar{u}_p , i.e., $t = X/\bar{u}_p$. Duty cycling in general results in an exponential decay of Φ^2 in time, with a decay rate that depends on τ_{on} and τ_{off} . The dashed red line is an exponential fit to the solid red curve of the simulation ($\tau_{off} = 0.4h/\bar{u}_p$, $\tau_{on} = 0.5h/\bar{u}_p$).

D. Optimum duty cycling protocols

We consider here two separate but related kinds of optimum duty cycles. The first involves identifying the duty cycle that maximizes the mixing incurred *per cycle*, equivalent to maximizing σ . This effectively minimizes the number of cycles required to achieve a target mixing quality, irrespective of the absolute cycle time required. The second kind of optimization attempts to achieve the fastest decay of Φ^2 per unit time, maximizing the quantity σ/τ_{cycle} without restricting the number of cycles required to achieve a targeted mixing quality. We show below that these two criteria in general result in different optimal protocols.

It is useful to interpret the action of the flow on a fluid element as a 2D mapping; each mapping results in some decay of the mix-variance Φ^2 , which occurs predominantly through mixing in the downstream vortex. The duty cycling allows the mapping to be repeatedly applied to the material volume, as it is transported past the bubble array. We have estimated in Sec. III B that the crossover time to less efficient, algebraic mix-variance decay occurs for $t^* \approx T_v^{\max}$; accordingly, we now postulate that the optimum “on” time should be given by

$$\tau_{on}^* \approx T_v^{\max}. \quad (12)$$

A shorter $\tau_{on} < \tau_{on}^*$ does not fully exploit the maximum shear χ_v^{\max} in the flow, while a longer $\tau_{on} > \tau_{on}^*$ results in less efficient algebraic stirring.

How should the “off” part of the cycle time be optimized? Its role is to ensure transport of fluid elements to the next downstream vortex such that it can mix with maximum efficiency. In particular, that means striation orientation should be transverse to the principal shear directions of that vortex. This condition of transversality (“streamline crossing”) has been investigated in detail in the context of linked-twist maps (LTMs) [17,60] with the most prominent example being the blinking vortex flow [15,61,62]. In such examples, one of two alternating flows stretches and simultaneously reorients striation elements such that the other flow can stretch them most efficiently. In direct analogy to LTM

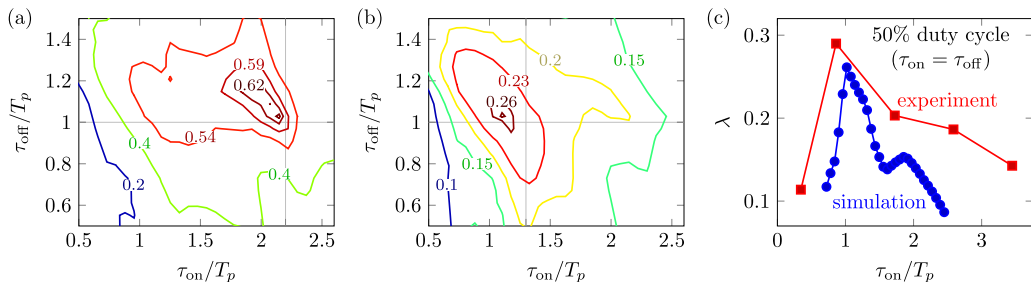


FIG. 6. Contours of the decay exponents of Φ^2 , (a) σ , and (b) λ , as a functions of τ_{on} and τ_{off} . Maximum values of σ and λ correspond respectively to duty cycling protocols that achieve optimum mixing per cycle and per unit time. The results shown here are for $h/a = 6.25$, $f = 21.9$ kHz, and $s = 0.02$ in a bubble array with a spacing of $L = 2h$ between bubbles. The simulations are run for a time $\approx 14T_p$ for each duty cycle. The horizontal and vertical gray lines in (a) and (b) give the analytical estimates from (12) and (13) (i.e., $\tau_{\text{on}} = \tau_{\text{on}}^* \approx T_v^{\text{max}}$ and $\tau_{\text{off}} = \tau_{\text{off}}^* \approx T_p$ for $\sigma_{\text{max}} \approx 0.69$), and the result of maximizing (16) (i.e., $\tau_{\text{on}} \approx 0.6T_v^{\text{max}} \approx 1.3T_p$ and $\tau_{\text{off}} \approx \tau_{\text{off}}^* \approx T_p$ for $\lambda_{\text{max}} \approx 0.25$). (c) Comparison of decay rates λ in experiments (red squares) and simulations (blue circles) for 50% duty cycling ($\tau_{\text{on}} = \tau_{\text{off}}$), showing a peak near $\tau_{\text{on}} \approx \tau_{\text{off}} \approx T_p$.

flows, we interpret the upstream vortex as the reorienting flow for the downstream vortex mixing. This means that the optimum configuration should transport fluid from the location of the upstream vortex to that of the downstream vortex during τ_{off} ,

$$\tau_{\text{off}}^* \approx T_p \equiv \frac{d_{vv}}{u_p}, \quad (13)$$

where T_p is the time required by the mean Poiseuille flow to transport fluid between the location of vortex centers a distance d_{vv} apart. A much smaller $\tau_{\text{off}} < T_p$ results in relatively small changes of the scalar field distribution between driving cycles. A larger $\tau_{\text{off}} > T_p$, however, causes fluid to flow past one (or both) of the vortices without being mixed. The geometry of microbubble streaming flow vortex centers is found to be insensitive to a wide range of driving frequency changes [36,38], with experiment and theory yielding a largely invariable vortex-to-vortex distance of $d_{vv} \approx 2.5a$.

It is convenient to normalize all relevant times by the transport time T_p ; we define a dimensionless ratio

$$\varphi \equiv \frac{T_v^{\text{max}}}{T_p}, \quad (14)$$

which is a property of the flow field (i.e., depends on s and f). Note that the ratio φ involves the orbit time on the maximally shearing closed streamline, the separation between vortices, and the mean speed of the Poiseuille flow. In the following, we will study in detail the mixing efficiency for a typical, practically relevant combination of $s = 0.02$ and $f = 21.9$ kHz; the resulting parameter value is $\varphi \approx 2.2$; cf. Fig. 3(a).

The duty cycle $\tau_{\text{on}} \approx T(\psi_{\text{max}})$ and $\tau_{\text{off}} \approx T_p$ is expected to result in the optimal use of vortices as well as the transport of fluid between them. This identifies the duty cycle that achieves the fastest mixing *per cycle*, i.e., it maximizes σ in (11). To estimate the maximum σ , we recall that the equation for vortical stirring (9) predicts a reduction of ϕ^2 by a factor of $\frac{1}{2}(1 + \phi_{\infty}^2)$ over the optimal stirring time T_v^{max} . If we assume that no further mixing takes place during the “off” part of the cycle, and that the duty cycling disrupts any unmixed regions so that ϕ_{∞}^2 becomes negligible after a few cycles, this factor translates to an ideal decay exponent $\sigma_{\text{max}} \simeq \log 2 = 0.69$. This prediction is in close agreement with the maximum value computed from simulations $\sigma \approx 0.65$, achieved when $\tau_{\text{on}} \approx 2.14T_p = 0.97T_v^{\text{max}}$ and $\tau_{\text{off}} \approx 1.15T_p$; cf. Fig. 6(a). It is worth noting that the theoretical optimum decay is the same as that obtained from a volume-preserving Baker’s transform [17]. The figure also shows that the estimates (12) and (13) for the optimum cycle times are very close to the

numerically determined optimum. We remark that σ_{\max} obtained from simulations is slightly smaller than the theoretical prediction, consistent with an initially nonzero ϕ_{∞}^2 .

The second optimum cycle of interest is the one that results in the fastest absolute decay of ϕ^2 per unit of time. We now recast (11) as

$$\phi_{\text{duty}}^2(t) = \alpha e^{-\lambda t/T_p}, \quad \text{where} \quad \lambda = \frac{\sigma T_p}{\tau_{\text{cycle}}}. \quad (15)$$

Here λ is a dimensionless decay rate per unit of time. In general, we expect the duty cycle that maximizes λ to differ from the one that maximizes σ due to a trade-off between the shorter cycle times ($\tau_{\text{cycle}} < T_p + T_v^{\max}$) and lower mixing efficiencies per cycle ($\sigma < \sigma_{\max}$), resulting in a mixing protocol that is ultimately faster in absolute time. We keep τ_{off} fixed at T_p , which is still the shortest “off” time that allows fluid to be transported between vortices, but now consider $\tau_{\text{on}} = \eta T_v^{\max}$, where $\eta < 1$ represents the fraction of T_v^{\max} for which the “on” part of the cycle is active. For any general $\tau_{\text{off}} = T_p$ and $\tau_{\text{on}} = \eta T_v^{\max}$, we can write $\sigma = \sigma(\eta)$, which has a maximum $\sigma_{\max} = \sigma(\eta = 1)$, i.e., when $\tau_{\text{on}} = T_v^{\max}$ and $\tau_{\text{off}} = T_p$ as discussed previously. By definition of a local maximum, $\sigma(\eta)$ must depend quadratically on $(\eta - 1)$ at leading order, i.e., $\sigma(\eta) - \sigma_{\max} \propto (\eta - 1)^2$. Assuming that no mixing (other than the negligible open-streamline mixing) occurs when $\tau_{\text{on}} = 0$ [i.e., $\sigma(\eta = 0) \approx 0$] we can write $\sigma(\eta) \simeq \eta(2 - \eta)\sigma_{\max}$ for $\tau_{\text{off}} = T_p$.

Using $\tau_{\text{cycle}} = T_p + \eta T_v^{\max}$ and the definitions of λ and φ yields

$$\lambda(\eta) \simeq \frac{\eta(2 - \eta)}{1 + \eta\varphi} \sigma_{\max} \quad \text{for} \quad \tau_{\text{off}} = T_p, \quad (16)$$

which is maximized when $\eta = (\sqrt{1 + 2\varphi} - 1)/\varphi$. For the value $\varphi = 2.2$ relevant to our flow, this optimal η corresponds to $\tau_{\text{on}} \approx 1.3T_p$ (i.e., $\eta \approx 0.6$) and a maximum decay rate $\lambda_{\max} \approx 0.25$. In simulations, we find that $\lambda_{\max} = 0.27$, realized when $\tau_{\text{off}} \approx 1.03T_p$ and $\tau_{\text{on}} = 1.14T_p$, once again in good agreement with the theoretical estimates, as indicated in Fig. 6(b). With simple approximations, we can thus predict both the optimum cycles and the decay exponents σ and λ obtained at these cycles.

We performed mixing experiments with 50% duty cycling ($\tau_{\text{on}} = \tau_{\text{off}}$) using a periodic array of bubbles. Values of ϕ^2 were calculated in periodic square ROIs located downstream of each bubble in the array. At each ROI location X (X measures distance along the array), ϕ^2 reaches a steady-state value (due to the continuous input of unmixed fluid), which is found to decay exponentially as $\phi^2 \propto \exp\{-\kappa X/(2h)\}$ where κ is the measured dimensionless spatial decay rate. To obtain an equivalent temporal decay rate that can be compared with the results of the simulations (periodic boundary conditions), we write $X \approx \bar{u}_p t$, thereby inferring an experimental temporal decay rate of $\lambda = \kappa \bar{u}_p/(2h)$. The experimentally inferred λ compares well with the results of the simulation (also sampled for $\tau_{\text{on}} = \tau_{\text{off}}$) and has a maximum value of ≈ 0.29 , realized when $\tau_{\text{on}} = \tau_{\text{off}} \approx 0.9T_p$. The decay rates in the experiments are somewhat greater than in the simulations, which can be attributed in part to diffusive mixing in experiments. In addition, we have assumed in the simulations that the steady streaming flow is 2D in nature, while it has been shown that microbubble streaming flows of this type do exhibit 3D flow effects (velocity components in the direction of the bubble axes) [40,63], which very likely enhance mixing.

Thus, we have shown that the theoretical predictions for the optimal duty cycle as well as the maximum decay rate σ^{\max} and λ^{\max} are in quantitative agreement with the results of both numerical simulations and experiments. The theoretical predictions follow from simple geometric and physical arguments and involve three distinct physical quantities: (1) the flow rate Q (the key measure of the transport flow throughput in a device), which manifests through \bar{u}_p , (2) the spacing between vortices d_{vv} (the key measure of the device geometry), and (3) the orbit time T_v^{\max} of the maximally shearing vortex streamline (the key measure of the vortex flow). These quantities are straightforward to calculate from the superposition flow $\mathbf{u}(\mathbf{x})$, requiring only the evaluation of simple integrals along closed steady orbits; cf. (8). Furthermore, these quantities have unambiguous meaning for any

open flow mixer with vortices and are not specific to bubble-based mixers. As a result, the theory circumvents the need to probe the entire 2D ($\tau_{\text{on}}, \tau_{\text{off}}$) space with unsteady mixing simulations or experiments in search of optimal duty cycling protocols in any given mixing device.

E. Diffusive effects

Even for large Péclet number, diffusive mixing ultimately becomes important as the advection field is further and further refined through the duty cycling. If the characteristic striation thickness in the bulk of the channel is $\ell_s(t)$, the time required to homogenize the mixture is of the order $\tau_D \sim \ell_s^2/D_p$. Further refinement of the advection field is only necessary if the effect of diffusion over the cycle time τ_{cycle} is negligible. Diffusion in the channel becomes important when $\tau_D \sim \tau_{\text{cycle}}$, or equivalently

$$\ell_s(t) \sim \sqrt{D_p \tau_{\text{cycle}}} \equiv \ell_1. \quad (17)$$

However, these striations are further thinned when the flow is squeezed through the narrow gap (which has thickness $d_{\text{gap}} \approx sh$) between the bubble and the upstream vortex as fluid elements are transported past the bubble [31,32]; cf. Fig. 1(c). By continuity, advective structures of size ℓ_s in the bulk channel are reduced to size $s\ell_s$ as they pass through the gap. The time required for diffusion to homogenize the fluid in the gap is therefore $\tau_{D,\text{gap}} \sim s^2 \ell_s^2/D_p$. On the other hand, the residence time of a fluid element within the gap is short, $\tau_{\text{gap}} \sim a/u_{\text{max}}$. For complete (diffusive) mixing within the gap, it is necessary that $\tau_{D,\text{gap}} \sim \tau_{\text{gap}}$, or

$$\ell_s(t) \sim \frac{1}{s} \sqrt{\frac{D_p a}{u_{\text{max}}}} = \sqrt{\frac{a}{s \tau_{\text{cycle}} \bar{u}_p}} \ell_1 \equiv \ell_2. \quad (18)$$

Bearing in mind that striation thicknesses decay in time, the relevant condition on the striation thickness $\ell(t)$ for complete diffusive mixing is set by the larger of ℓ_1 and ℓ_2 . For mixers with strong streaming vortices ($s \ll 1$), the optimal τ_{cycle} is not much greater than $T_p = d_{\text{vv}}/\bar{u}_p$ (here, the optimal $\tau_{\text{cycle}} \approx 3T_p$; see Fig. 5), so that $\ell_2 > \ell_1$ [see Eq. (18)], suggesting that diffusive mixing in the gap occurs for larger ℓ_s , or equivalently for earlier times, compared with diffusion in the bulk of the channel. As established before, $\Phi^2 \propto \ell_s$, so that the decay of a characteristic striation thickness follows that of the mix-variance, $\ell_s \sim \ell_0 \exp\{-\sigma t/\tau_{\text{cycle}}\}$. Assuming that the initial striation thickness is comparable to the channel height, the required residence time t_{res} in the mixer is

$$\frac{t_{\text{res}}}{\tau_{\text{cycle}}} \sim \frac{1}{\sigma} \log \left(sh \sqrt{\frac{u_{\text{max}}}{a D_p}} \right) = \frac{1}{2\sigma} \log \left(\frac{sh}{a} \text{Pe} \right). \quad (19)$$

For typical experimental conditions with $s \sim 0.02$ and $h/a = 6.25$, this corresponds to $\lesssim 6$ optimum duty cycles at $\text{Pe} \sim 10^5$ for complete diffusive mixing to occur.

We remark here that we have accounted for diffusion only in the simplest way possible: by assuming that it occurs independently from the advection. In practice, diffusive processes are enhanced due to the presence of flow gradients (Taylor–Aris dispersion) [11,55,56,64]. Additionally, the current approach takes into account the steady streaming flow only, resulting from a time average of oscillatory flow; flow oscillations on the faster time scale of the bubble oscillation further contribute to diffusive mixing [65]. It is then to be expected that the typical residence time required in practice is smaller than the t_{res} estimated here.

IV. CONCLUSIONS

In the present work, we have investigated 2D advective mixing strategies under continuous throughput of the species to be mixed, using locally actuated vortex structures. In this application-relevant scenario, the mixing effectiveness of steady flow actuation is severely limited; the presence of recirculation regions in the flow (1) inhibits the transport of fluid, and (2) produces only slow,

algebraic mixing at long times. Both of these limitations are overcome by the deliberate introduction of flow unsteadiness, e.g., by duty cycling the vortex activity. For the example of ultrasound-driven microbubble arrays, this is easily realized by a modulation of the driving voltage, and we have quantified the resulting mixing in experiments and simulations, finding agreement with the following general results of our theoretical analysis.

Under duty-cycle flow modulation, the quality of mixing—quantified by the mix-variance of the advection pattern—decays exponentially with time (or equivalently the number of cycles), with the decay exponent being dependent on the duty cycle chosen. The optimum duty cycle is shown to be one that (1) optimally uses the vortical regions of the flow for stirring during the “on” part of the cycle and (2) optimally transports the stirred fluid between vortices during the “off” part of the cycle. The optimization parameters of the flow modulation are understood from general transport properties in regions of closed and open flow lines, making direct use of concepts previously developed in idealized closed-volume mixing. Knowledge of the flow rate, the vortex spacing, and a characteristic vortex turnover time is sufficient to predict optimum duty-cycle parameters. This constitutes the first systematic study of flow modulation protocols for optimal micromixing under continuous transport of fluid through a microchannel, a practical constraint in most micromixing applications. The approach is not confined to bubble microstreaming, but is applicable to any flow that combines transport with local vortex actuation.

The results pertain to advective mixing (stirring); the mixture is ultimately homogenized by diffusion, which sets the required residence time in the mixer for a given particle size. For typical experimental parameters of bubble microstreaming, the decisive diffusive processes are expected to occur in the narrow gap between the bubble and the upstream vortex. We emphasize that the time scales estimated in the present work are a “worst-case” scenario, with practical mixing times likely to be shorter: We have separated the advective and diffusive processes here, while in practice, the diffusion of the scalar field occurs simultaneously with advection, and is generally enhanced by the gradients of the flow (Taylor–Aris dispersion) on both steady and oscillatory time scales. Additionally, 3D flow effects that have been neglected here but can be excited in microbubble streaming setups are likely to improve mixing. Despite these simplifying assumptions, the present work provides useful estimates for the systematic understanding and practical design of open flow micromixing devices.

ACKNOWLEDGMENTS

The authors acknowledge support by the National Science Foundation for this work under Grant No. CBET-1236141. B.R. acknowledges partial support from the Carbon Mitigation Initiative of Princeton University. We thank Lin Guo for preliminary simulations and Emmanuel Villiermaux and Igor Mezić for stimulating conversations.

-
- [1] E. L. Shock and M. D. Schulte, Organic synthesis during fluid mixing in hydrothermal systems, *J. Geophys. Res. Planets* **103**, 28513 (1998).
 - [2] J. M. Ottino, *The Kinematics of Mixing: Stretching, Chaos, and Transport* (Cambridge University Press, Cambridge, 1989).
 - [3] M. Kakuta, F. G. Bessoth, and A. Manz, Microfabricated devices for fluid mixing and their application for chemical synthesis, *Chem. Record* **1**, 395 (2001).
 - [4] J. M. Ottino, Mixing, chaotic advection, and turbulence, *Annu. Rev. Fluid Mech.* **22**, 207 (1990).
 - [5] E. Villiermaux and J. Duplat, Mixing as an Aggregation Process, *Phys. Rev. Lett.* **91**, 184501 (2003).
 - [6] E. Villiermaux, Unifying ideas on mixing and atomization, *New J. Phys.* **6**, 125 (2004).
 - [7] N.-T. Nguyen and Z. Wu, Micromixers—A review, *J. Micromech. Microeng.* **15**, R1 (2005).

- [8] E. Villermaux and C. Innocenti, On the geometry of turbulent mixing, *J. Fluid Mech.* **393**, 123 (1999).
- [9] A. D. Stroock, S. K. W. Dertinger, A. Ajdari, I. Mezić, H. A. Stone, and G. M. Whitesides, Chaotic mixer for microchannels, *Science* **295**, 647 (2002).
- [10] J. M. Ottino and S. Wiggins, Introduction: Mixing in microfluidics, *Philos. Trans. Roy. Soc. Lond. A* **362**, 923 (2004).
- [11] R. F. Ismagilov, A. D. Stroock, P. J. A. Kenis, G. Whitesides, and H. A. Stone, Experimental and theoretical scaling laws for transverse diffusive broadening in two-phase laminar flows in microchannels, *Appl. Phys. Lett.* **76**, 2376 (2000).
- [12] T. M. Antonsen, Jr., Z. Fan, E. Ott, and E. Garcia-Lopez, The role of chaotic orbits in the determination of power spectra of passive scalars, *Phys. Fluids* **8**, 3094 (1996).
- [13] P. Tabeling, M. Chabert, A. Dodge, C. Jullien, and F. Okkels, Chaotic mixing in cross-channel micromixers, *Philos. Trans. Roy. Soc. Lond. A* **362**, 987 (2004).
- [14] Z. Lin, J.-L. Thiffeault, and C. R. Doering, Optimal stirring strategies for passive scalar mixing, *J. Fluid Mech.* **675**, 465 (2011).
- [15] H. Aref, Stirring by chaotic advection, *J. Fluid Mech.* **143**, 1 (1984).
- [16] R. Burton and R. W. Easton, in *Ergodicity of Linked Twist Maps* (Springer, Berlin, 1980), pp. 35–49.
- [17] R. Sturman, J. M. Ottino, and S. Wiggins, *The Mathematical Foundations of Mixing* (Cambridge University Press, Cambridge, 2006).
- [18] A. P. Sudarsan and V. M. Ugaz, Multivortex micromixing, *Proc. Natl. Acad. Sci. USA* **103**, 7228 (2006).
- [19] J. Melin, G. Giménez, N. Roxhed, W. van der Wijngaart, and G. Stemme, A fast passive and planar liquid sample micromixer, *Lab Chip* **4**, 214 (2004).
- [20] H.-Y. Lee and J. Voldman, Optimizing micromixer design for enhancing dielectrophoretic microconcentrator performance, *Anal. Chem.* **79**, 1833 (2007).
- [21] M. H. Oddy, J. G. Santiago, and J. C. Mikkelsen, Electrokinetic instability micromixing, *Anal. Chem.* **73**, 5822 (2001).
- [22] P.-H. Huang, Y. Xie, D. Ahmed, J. Rufo, N. Nama, Y. Chen, C. Y. Chan, and T. J. Huang, An acoustofluidic micromixer based on oscillating sidewall sharp-edges, *Lab Chip* **13**, 3847 (2013).
- [23] P.-H. Huang, N. Nama, Z. Mao, P. Li, J. Rufo, Y. Chen, Y. Xie, C.-H. Wei, L. Wang, and T. J. Huang, A reliable and programmable acoustofluidic pump powered by oscillating sharp-edge structures, *Lab Chip* **14**, 4319 (2014).
- [24] P. Agrawal, P. S. Gandhi, and A. Neild, Particle manipulation affected by streaming flows in vertically actuated open rectangular chambers, *Phys. Fluids* **28**, 032001 (2016).
- [25] D. J. Collins, Z. Ma, J. Han, and Y. Ai, Continuous micro-vortex-based nanoparticle manipulation via focused surface acoustic waves, *Lab Chip* **17**, 91 (2017).
- [26] D. J. Collins, B. L. Khoo, Z. Ma, A. Winkler, R. Weser, H. Schmidt, J. Han, and Y. Ai, Selective particle and cell capture in a continuous flow using micro-vortex acoustic streaming, *Lab Chip* **17**, 1769 (2017).
- [27] J. A. Levitan, S. Devasenathipathy, V. Studer, Y. Ben, T. Thorsen, T. M. Squires, and M. Z. Bazant, Experimental observation of induced-charge electro-osmosis around a metal wire in a microchannel, *Colloids Surf. A* **267**, 122 (2005).
- [28] C. Canpolat, M. Zhang, W. Rosen, S. Qian, and A. Beskok, Induced-charge electroosmosis around touching metal rods, *J. Fluids Eng.* **135**, 021103 (2013).
- [29] C. Park and S. T. Wereley, Rapid generation and manipulation of microfluidic vortex flows induced by ac electrokinetics with optical illumination, *Lab Chip* **13**, 1289 (2013).
- [30] P. Marmottant and S. Hilgenfeldt, Controlled vesicle deformation and lysis by single oscillating bubbles, *Nature (London)* **423**, 153 (2003).
- [31] C. Wang, S. V. Jalikop, and S. Hilgenfeldt, Size-sensitive sorting of microparticles through control of flow geometry, *Appl. Phys. Lett.* **99**, 034101 (2011).
- [32] C. Wang, S. V. Jalikop, and S. Hilgenfeldt, Efficient manipulation of microparticles in bubble streaming flows, *Biomicrofluid.* **6**, 012801 (2012).
- [33] R. Thameem, B. Rallabandi, and S. Hilgenfeldt, Particle migration and sorting in microbubble streaming flows, *Biomicrofluid.* **10**, 014124 (2016).

- [34] R. H. Liu, J. Yang, M. Z. Pindera, M. Athavale, and P. Grodzinski, Bubble-induced acoustic micromixing, *Lab Chip* **2**, 151 (2002).
- [35] D. Ahmed, X. Mao, B. K. Juluri, and T. J. Huang, A fast microfluidic mixer based on acoustically driven sidewall-trapped microbubbles, *Microfluid. Nanofluid.* **7**, 727 (2009).
- [36] C. Wang, B. Rallabandi, and S. Hilgenfeldt, Frequency dependence and frequency control of microbubble streaming flows, *Phys. Fluids* **25**, 022002 (2013).
- [37] N. Bertin, T. A. Spelman, T. Combriat, H. Hue, O. Stéphan, E. Lauga, and P. Marmottant, Bubble-based acoustic micropulsors: Active surfaces and mixers, *Lab Chip* **17**, 1515 (2017).
- [38] B. Rallabandi, C. Wang, and S. Hilgenfeldt, Two-dimensional streaming flows driven by sessile semicylindrical microbubbles, *J. Fluid Mech.* **739**, 57 (2014).
- [39] C. Wang, Microbubble streaming flows for non-invasive particle manipulation and liquid mixing, Ph.D. thesis, University of Illinois at Urbana-Champaign (2013).
- [40] A. Marin, M. Rossi, B. Rallabandi, C. Wang, S. Hilgenfeldt, and C. J. Kähler, Three-Dimensional Phenomena in Microbubble Acoustic Streaming, *Phys. Rev. Appl.* **3**, 041001 (2015).
- [41] S. M. Davidson, M. Wessling, and A. Mani, On the dynamical regimes of pattern-accelerated electroconvection, *Sci. Rep.* **6**, 22505 (2016).
- [42] J. C. McDonald, D. C. Duffy, J. R. Anderson, D. T. Chiu, H. Wu, O. J. A. Schueller, and G. M. Whitesides, Fabrication of microfluidic systems in poly(dimethylsiloxane), *Electrophoresis* **21**, 27 (2000).
- [43] F. Bottausci, C. Cardonne, C. Meinhart, and I. Mezić, An ultrashort mixing length micromixer: The shear superposition micromixer, *Lab Chip* **7**, 396 (2007).
- [44] J. Aubin, M. Ferrando, and V. Jiricny, Current methods for characterising mixing and flow in microchannels, *Chem. Eng. Sci.* **65**, 2065 (2010).
- [45] D. Gobby, P. Angeli, and A. Gavrilidis, Mixing characteristics of T-type microfluidic mixers, *J. Micromech. Microeng.* **11**, 126 (2001).
- [46] S. S. Wang, Z. J. Jiao, X. Y. Huang, C. Yang, and N. T. Nguyen, Acoustically induced bubbles in a microfluidic channel for mixing enhancement, *Microfluid. Nanofluid.* **6**, 847 (2009).
- [47] N. Riley, Steady streaming, *Annu. Rev. Fluid Mech.* **33**, 43 (2001).
- [48] N. A. Mortensen, F. Okkels, and H. Bruus, Reexamination of Hagen-Poiseuille flow: Shape dependence of the hydraulic resistance in microchannels, *Phys. Rev. E* **71**, 057301 (2005).
- [49] R. Thameem, Quantifying particle sorting in microbubble streaming flows, Master's thesis, University of Illinois at Urbana-Champaign (2015).
- [50] L. Cortelezzi, A. Adrover, and M. Giona, Feasibility, efficiency and transportability of short-horizon optimal mixing protocols, *J. Fluid Mech.* **597**, 199 (2008).
- [51] O. Gubanov and L. Cortelezzi, Towards the design of an optimal mixer, *J. Fluid Mech.* **651**, 27 (2010).
- [52] D. Saintillan and M. J. Shelley, Emergence of coherent structures and large-scale flows in motile suspensions, *J. Roy. Soc. Interface* **9**, 571 (2012).
- [53] G. Mathew, I. Mezić, and L. Petzold, A multiscale measure for mixing, *Physica D* **211**, 23 (2005).
- [54] G. Mathew, I. Mezić, S. Grivopoulos, U. Vaidya, and L. Petzold, Optimal control of mixing in stokes fluid flows, *J. Fluid Mech.* **580**, 261 (2007).
- [55] G. I. Taylor, Dispersion of soluble matter in solvent flowing slowly through a tube, *Proc. Roy. Soc. A* **219**, 186 (1953).
- [56] R. Aris, On the dispersion of a solute in a fluid flowing through a tube, *Proc. Roy. Soc. A* **235**, 67 (1956).
- [57] S. Wiggins, *Introduction to Applied Nonlinear Dynamical Systems and Chaos* (Springer Science & Business Media, New York, 2003), Vol. 2.
- [58] P. Meunier and E. Villermaux, How vortices mix, *J. Fluid Mech.* **476**, 213 (2003).
- [59] J.-L. Thiffeault, Using multiscale norms to quantify mixing and transport, *Nonlinearity* **25**, R1 (2012).
- [60] S. Wiggins and J. M. Ottino, Foundations of chaotic mixing, *Philos. Trans. Roy. Soc. Lond. A* **362**, 937 (2004).
- [61] D. V. Khakhar, H. Rising, and J. M. Ottino, Analysis of chaotic mixing in two model systems, *J. Fluid Mech.* **172**, 419 (1986).
- [62] V. V. Meleshko and H. Aref, A blinking rotlet model for chaotic advection, *Phys. Fluids* **8**, 3215 (1996).

- [63] B. Rallabandi, A. Marin, M. Rossi, C. J. Kähler, and S. Hilgenfeldt, Three-dimensional streaming flow in confined geometries, *J. Fluid Mech.* **777**, 408 (2015).
- [64] P. B. Rhines and W. R. Young, How rapidly is a passive scalar mixed within closed streamlines? *J. Fluid Mech.* **133**, 133 (1983).
- [65] E. J. Watson, Diffusion in oscillatory pipe flow, *J. Fluid Mech.* **133**, 233 (1983).